Journal of Membrane Science 627 (2021) 119241

Contents lists available at ScienceDirect

Journal of Membrane Science

journal homepage: http://www.elsevier.com/locate/memsci

Carbon molecular sieve membranes for hydrogen purification from a steam methane reforming process

Linfeng Lei [a], Arne Lindbråthen [a], Magne Hillestad [a,**], Xuezhong He [b,c,*]

[a] Department of Chemical Engineering, Norwegian University of Science and Technology, NO-7491, Trondheim, Norway
[b] Department of Chemical Engineering, Guangdong Technion Israel Institute of Technology (GTIIT), 241 Daxue Road, Shantou 515063, China
[c] The Wolfson Department of Chemical Engineering, Technion - Israel Institute of Technology, Haifa 32000, Israel

ARTICLE INFO

Keywords:
Carbon molecular sieve membranes
Hydrogen purification
Steam methane reforming
Process simulation
Gas separation

ABSTRACT

Asymmetric carbon molecular sieve (CMS) membranes prepared from cellulose hollow fiber precursors were investigated for H_2/CO_2 separation in this work. The prepared carbon membrane shows excellent separation performance with H_2 permeance of 111 GPU and an H_2/CO_2 selectivity of 36.9 at 10 bar and 110 °C dry mixed gas. This membrane demonstrates high stability under a humidified gas condition at 90 °C and the pressure of up to 14 bar. A two-stage carbon membrane system was evaluated to be techno-economically feasible to produce high-purity H_2 (>99.5 vol%) by HYSYS simulation, and the minimum specific H_2 purification cost of 0.012 $/Nm^3 H_2 produced was achieved under the optimal operating condition. Sensitivity analysis on the H_2 loss and H_2 purity indicates that such membrane is still less cost-effective to achieve ultrapure hydrogen (e.g., >99.8 vol %) unless the higher operating temperatures for carbon membrane systems are applied.

1. Introduction

Hydrogen production from natural gas (NG) is the most applied technology, which has been a suitable approach for implementing the hydrogen economy concerning low-carbon energy future and the reduction of greenhouse gas emissions [1,2]. Steam methane reforming (SMR) process integrated with water-gas shift (WGS) reactor is widely used for the efficient conversion of NG to hydrogen. However, the produced H_2 stream usually contains a significant amount of CO_2 that should be removed to produce high purity hydrogen. Purification of hydrogen from this gas stream requires novel separation technologies to improve energy efficiency as it consumes ca. 60% of the total energy requirement in the whole hydrogen production process. The state-of-the-art hydrogen purification technologies of pressure swing adsorption (PSA) and cryogenic distillation [2–4] are energy-intensive, while membrane gas separation technology shows its potential in this application because of its high energy efficiency, small footprint, and process flexibility. Different types of membranes such as palladium membranes [5], polymeric membranes [6,7], two-dimensional (2D) nanosheets [8,9], mixed matrix membranes [10,11], and carbon membranes [12] have been investigated for H_2/CO_2 separation. Although great effort has been put into the development of palladium-based membranes for the production of high-purity H_2 for fuel cells [5], the cost of palladium membranes is still high, which cannot yet compete with PSA. In comparison, the polymeric and mixed matrix membranes have the challenges to endure adverse conditions (e.g., high temperature and pressure), which limits the membrane stability under such circumstances.

Carbon molecular sieve (CMS) membranes, consisting of rigid pore structures, have great advantages of strong mechanical and chemical stabilities and are considered promising candidates for the high-temperature and -pressure demanded scenarios. Carbon membranes can be fabricated into a hollow fiber configuration which is suitable for making membrane modules with high packaging density for large-scale applications. Due to a bimodal pore structure with ultramicropores and micropores, CMS membranes present high separation performance that can exceed the Robeson upper bound (2008) [13] to reach the industrial attractive region for this application [14]. Different polymeric precursors, such as cellulose derivatives [15–17], polyimide [18–20], poly (vinylidene fluoride) (PVDF) [21], and polyacrylonitrile (PAN) [22], have been employed to prepare CMS membranes for various gas separations. Supported CMS membranes integrated into membrane reactors

* Corresponding author. Department of Chemical Engineering, Guangdong Technion Israel Institute of Technology (GTIIT), 241 Daxue Road, Shantou 515063, China.
** Corresponding author.
E-mail addresses: magne.hillestad@ntnu.no (M. Hillestad), xuezhong.he@gtiit.edu.cn (X. He).

https://doi.org/10.1016/j.memsci.2021.119241
Received 5 January 2021; Received in revised form 10 February 2021; Accepted 28 February 2021
Available online 5 March 2021

for hydrogen production have been investigated by the Tsotsis group [23–25]. They reported good stability of CMS membranes when it is operated at the temperatures and pressures of up to 250 °C and 25 bar, respectively. However, achieving a high H_2/CO_2 selectivity is still challenging due to the presence of a selective surface flow (SSF) transport mechanism for CO_2 molecules that allows a significant amount of CO_2 molecules to pass through the membranes. To overcome this predicament, tuning the ultramicropores of CMS membranes to a narrower size (e.g., 3–4 Å) that restricts CO_2 diffusion, could be an effective method to improve the H_2/CO_2 selectivity by switching to the molecular sieving dominated mechanism. A facile approach by elevating carbonization temperature to enhance the H_2/CO_2 selectivity has been reported by Zhang et al. [26]. The H_2/CO_2 selectivity was increased from 3 to 11 when the carbonization temperature was raised from 750 to 900 °C. However, there was a large concomitant decrease in H_2 permeability from 1600 to 240 barrer, which corresponds to a reduction in H_2 permeance from 65 to 10 GPU (estimated from the reported thickness of ca. 25 μm) [26]. Such a significant reduction in gas permeance will dramatically increase the capital cost due to the larger required membrane area, which may not offset the reduced operating cost with the enhanced selectivity to complete a specific separation task. Thus, the preparation of CMS membranes with asymmetric structure (i.e., a dense selective layer and an integral porous inner support layer) may provide a relatively lower transport resistance and thereby potentially offset the gas permeance drop when they are prepared at a higher carbonization temperature [18,27].

In the current work, high-performance asymmetric carbon hollow fiber membranes (CHFMs) were prepared by carbonization of the cellulose hollow fiber precursors spun from a cellulose/ionic liquid dope solution. By controlling the spinning conditions, the asymmetric cellulose hollow fiber precursors were obtained and further carbonized at 700 °C to produce asymmetric CHFMs. The procedure does not require any additional crosslinking treatment, which has often been used in the preparation of asymmetric carbon membranes to avoid pore collapse during the carbonization. The prepared CHFMs were evaluated by feeding a mixed gas of 50 vol% H_2/50 vol% CO_2 under different temperatures (up to 110 °C) and pressures (up to 14 bar). Permeation testing under a 100% relative humidity (RH) mixed gas at 90 °C indicates that the cellulose-based CHFMs have good stability under the water-vapor exposed conditions. The great advantage of the water-vapor resistance capability for the cellulose-based CMS membranes also shows a promising opportunity for other separation scenarios where water vapor exists. Techno-economic feasibility of a two-stage membrane system for the production of high purity H_2 (>99.5 vol%) from a feed gas of 6000 kmol/h was conducted by HYSYS simulation based on the measured membrane performance. The operating conditions, such as feed and permeate pressures, were optimized to achieve a minimum specific H_2 purification cost.

2. Method

2.1. Membrane preparation

Cellulose hollow fiber precursors were fabricated by a dry-wet spinning process. The 12 wt % microcrystal cellulose (MCC, Avicel PH-101, purchased from Sigma-Aldrich) was dissolved in a cosolvent of 1-Ethyl-3-methylimidazolium Acetate (EmimAc, > 95%, purchased from IOLITEC GmbH) and dimethyl sulfoxide (DMSO, FCC grade, purchased from Sigma-Aldrich) with a weight ratio of 3:1 for EmimAc: DMSO as the dope solution for spinning. Bore solution of 80 wt% cosolvent and 20 wt% non-solvent of water was used. Moreover, water was used as a coagulation fluid, and the temperature of the first and second coagulation bath was controlled at 60 °C and 40 °C, respectively. The nascent water-wetted cellulose hollow fibers were then immersed into isopropanol (≥99.7%, FCC grade, purchased from Sigma-Aldrich) and followed with *n*-hexane (ReagentPlus®, ≥99%, purchased from Sigma-Aldrich) for the solvent exchange to maintain the obtained asymmetric structure. Afterward, the CHFMs were prepared by the carbonization of asymmetric cellulose hollow fibers with the argon purge gas using the carbonization procedure described in the previous work [30]. In brief, the cellulose precursors were initially heated from room temperature up to 200 °C at a heating rate of 10 °C/min and followed by a 4 °C/min from 200 to 300 °C. After an isothermal dwell at 300 °C for 120 min, a heating rate of 5 °C/min was applied to reach the final carbonization temperature of 700 °C for preparing the desired carbon membranes. The average outer diameter and the thickness of the selective layer for the prepared carbon membranes are ca. 215 μm and 3 μm, respectively, as is shown in the SEM image in Fig. 1a. In total 10 carbon hollow fiber membranes were mounted into a lab-scale module (3/8-inch stainless steel tubing) with an effective membrane area of 9 cm^2 (See Fig. 1b and c for the illustrations of the construction for membrane module and a photograph of the testing module, respectively). Both sides of the module are open, and the CHFMs are evenly arranged inside the tubing to get a well-distributed gas flow pattern and are sealed by the Loctite EA 3430 epoxy adhesive. The prepared lab-scale module was tested with the mixed gas permeation rig to document the membrane separation performance (see Fig. 1d).

2.2. Mixed gas permeation testing

In this work, the prepared carbon membrane module was tested with a fully-humidified (100% RH) pre-mixed gas of 50 vol% H_2/50 vol% CO_2 at different feed pressures of 8–14 bar at 90 °C to document the feed pressure influence on the membrane separation performance and the membrane stability of moisture exposure. Moreover, the same module was also tested at various temperatures of 25–110 °C using a 150 Nml/min dry mixed gas at a constant feed pressure of 10 bar. The sweep gas of argon is used in the permeate side at 1 bar with a flow rate of 50 Nml/min, which provides sufficiently high flow for the gas chromatograph (GC, 8610C, SRI Instruments Inc.) analysis. An illustration of the mixed gas permeation rig is depicted in Fig. 1d. For all the experiments, the gas mixture was fed from the shell side of the module, and hydrogen permeates through the carbon membranes to the bore side. The permeate gas composition of H_2 and CO_2 was analyzed by GC, while the total permeate flow was measured by an online bubble flow meter (see Fig. 1d). Gas permeance (*Pe*) is calculated by Eq. (1),

$$Pe_i = \frac{J_i}{\Delta p_i} = \frac{q_i}{A \cdot \Delta p_i} \tag{1}$$

Where J_i (m^3(STP)/(m^2·h) and q_i (m^3(STP)/h) are the permeate flux and flow rate of the gas component *i* ($q_i = q \times y_i$, where *q* is the total permeate flow rate (m^3(STP)/h)). *A* and Δp_i are the effective membrane area (m^2) and partial pressure difference (bar) of component *i*, respectively. The driving force of component *i* is then calculated by ($\Delta P_i = x_i \times P_F - y_i \times p_P$), where P_F, and p_P are the total feed and permeate pressures. The separation factor is calculated by $S_{i/j} = \frac{y_i/y_j}{x_i/x_j}$, in which *x* and *y* are the concentrations of the components *i* and *j* in the feed and permeate, respectively.

2.3. Process evaluation

2.3.1. Process description and design

In a hydrogen plant, natural gas is preheated and mixed with a small hydrogen stream before it enters a desulphurization unit. Steam is added and further heated to ca. 400 °C and fed to a pre-reformer, where higher hydrocarbons are converted to methane. This is to prevent coking in the steam-methane reformer. The gas is further heated to ca. 500 °C before it is fed to the reformer tubes where methane and steam react to form CO and hydrogen. The resulted gas consists of hydrogen, CO, CO_2, water, and some inert, and is further cooled down to 350–400 °C before it is fed to a high-temperature shift reactor. A typical product stream composes

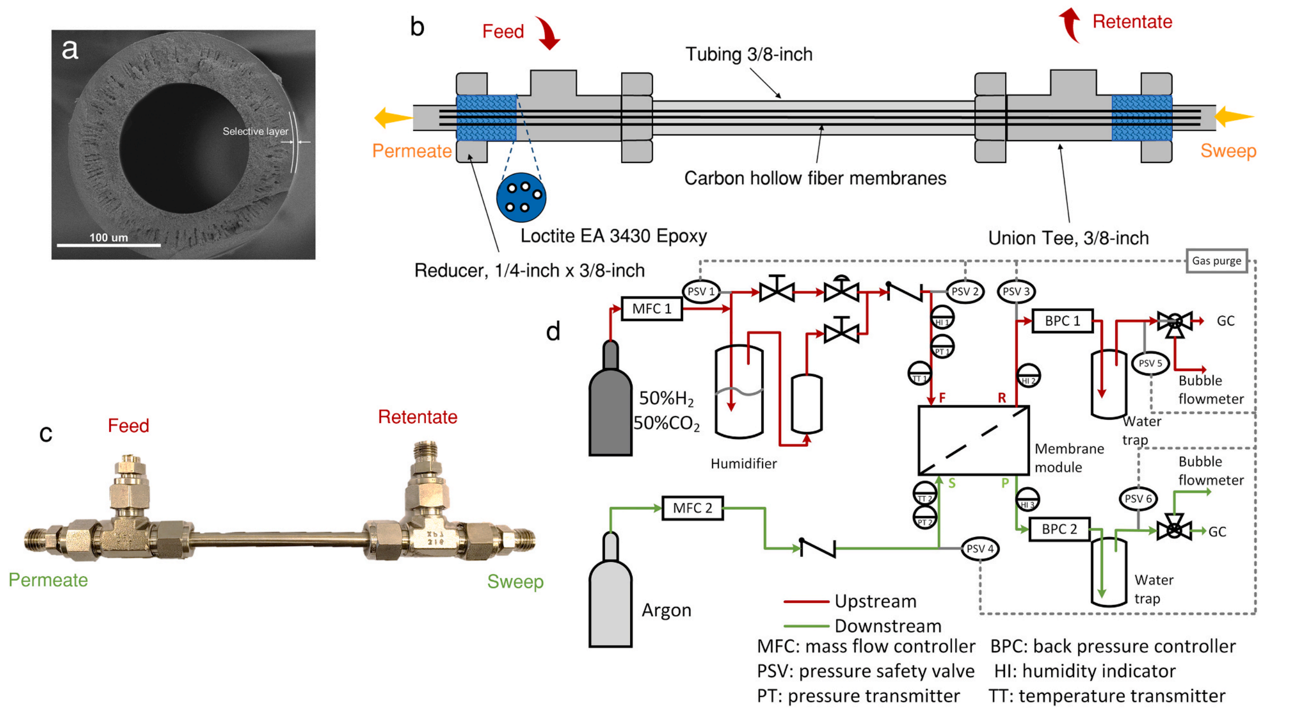

Fig. 1. a) SEM image of the prepared carbon hollow fiber membrane, b) an illustration of the CHFM module in a counter-current flow pattern, c) a photograph of a CHFM module for mixed gas permeation testing, and d) schematic of the mixed gas permeation rig.

H_2, CO_2, CH_4, and CO, and a second shift process involving a low-temperature water-gas shift (LTWGS) reaction is often used to fully convert CO to CO_2. The outlet gas consists of mainly hydrogen and CO_2, with a small amount of unconverted CO and methane. The stream out of the LTWGS reactor is cooled to 100–200 °C before it goes into the membrane system where the CO_2 and other impurities (like CH_4, CO, H_2O, HCs) are separated from hydrogen. It should be noted that the gas permeances of CO, CH_4 and HCs are usually much lower compared to CO_2 and will stay together with the enriched CO_2 stream in the retentate. Therefore, the main components CO_2, H_2, H_2O are only considered to simplify the process simulation as listed in Table 1.

A two-stage carbon membrane system for H_2 purification was designed, as illustrated in Fig. 2. The 1st-stage is designed to control the H_2 loss (<10%) by adjusting the membrane area together with the 2nd-stage retentate recycling. Simultaneously, the 2nd-stage membrane unit will produce high purity H_2 (>99.5 vol%) based on the required membrane area under the given operating conditions, which is particularly interested in being used as the H_2 source for downstream petrochemical industries and/or catalytic conversion to chemicals/fuels.

The gas stream that comes out from the LTWGS reactor will be dehydrated to remove most of the water vapor. The relatively dry gas is then fed into the 1st-stage membrane unit (M − 1) after it is pre-heated to a given operating temperature (e.g., 100–200 °C) for carbon membranes. Heat exchange network has not been considered in this work, which can be conducted by the heat integration between the condenser (C-1) and the heat exchanger (E−1) in future work. The 1st-stage permeate stream containing the enriched H_2 is compressed (inter-stage compressor: K-1) and sent to the 2nd-stage carbon membrane unit (M − 2) for the ultimate purification to produce high purity hydrogen (>99.5 vol%). While the 2nd-stage retentate is recycled back to the 1st-stage feed to avoid a high H_2 loss, and the additional compressor (K-2) might be applied if the feed pressure of the 2nd-stage is lower than that of the 1st-stage.

Table 1
Characteristics of products from integrated SMR + LTWGS processes.

Parameter	Value
Feed gas flow rate, kmol/h	6000–8000
Temperature, °C	200
Pressure, bar	10–20
Gas composition[a], vol. %	
CO_2	19
H_2	61
H_2O	20

[a] The impurities of CO and CH_4 are not included.

2.3.2. *Simulation basis*

To document the technological and economic feasibility of carbon membrane systems for H_2 purification from a steam methane reforming process, the simulation basis listed in Table 2 was chosen based on the experimental data obtained in this work and the process condition described above. Extrapolation of the experimental results is employed to model the scenarios that were not tested in the experiments, which is described in section 3.1. It should be noted that the H_2O permeance cannot be measured in the experiment due to the difficulty of determining the water concentration in the permeate gas stream using GC. Since the H_2 diffusion coefficient would be expected to be close to H_2O given their similar kinetic diameters, whereas H_2O sorption on cellulose-derived carbon membranes is strong as reported by Rodrigues et al. [28], so it is suspected that the water vapor permeance through the developed carbon membranes could be higher compared with hydrogen, as reported by Sá et al. [29]. However, increasing operating temperature is expected to reduce the water adsorption on the carbon matrix, therefore, we assume that water vapor permeance is the same as H_2 in this work due to the high operating temperatures in a steam methane reformation process. Future work on testing the H_2O adsorption of this carbon membrane may provide more accurate data for simulation-this is however not included in the current work. It should be noted that our previous work has already reported the stability of this carbon membrane exposed to a humidified feed gas, and the stable performance was found over 120 h under a 100% RH humidified mixed gas at 10 bar and 90 °C [30]. Thus, the humidity influence on membrane performance was not

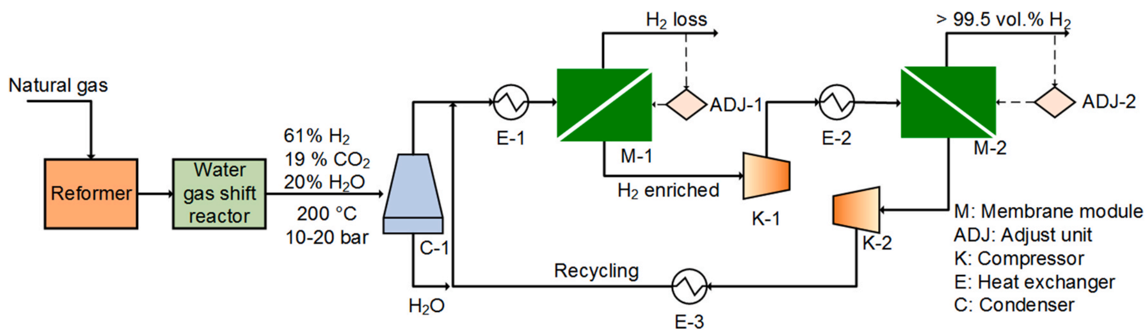

Fig. 2. Process flow diagram of a two-stage carbon membrane system for hydrogen purification in an SMR + WGS process.

Table 2
Simulation basis of a membrane system for H_2 purification.

Parameter	1st-stage	2nd-stage
Feed pressure, bar	Optimized	Optimized
Permeate pressure, bar	Optimized	1
Temperature, °C	90–200	90–200
H_2 permeance, $m^3(STP)/(m^2 \cdot h \cdot bar)$	Experimental data (Figs. 3 and 4)	
H_2O permeance, $m^3(STP)/(m^2 \cdot h \cdot bar)$	Assuming the same as H_2	
H_2/CO_2 selectivity	Experimental data (Figs. 3 and 4)	
Total H_2 loss, %	<10	
H_2 purity, vol%		>99.5

considered in this work. The previously reported method on process simulation of carbon membranes for gas separation and purification [26,31] was introduced in this work. The designed two-stage carbon membrane system was simulated by HYSYS integrated with a ChemBrane model (in-house membrane model [31]) to document the technological feasibility. The gas permeation through the carbon hollow fiber membranes in a counter-current plug flow pattern with shell side feeding was described in the previous work [31]. It should be noted that the ChemBrane model does not separately consider the transport in the surface adsorption phase and the bulk diffusion phase, instead the overall mass transfer coefficient is represented by the apparent gas permeance, which considers both the competing diffusion and sorption effect of gas components transporting through carbon membranes. It is worth noting that the simulation results based on the ChemBrane model have been compared with the experimental data and presented a good consistency as reported in the previous work [32]. Therefore, this membrane model was introduced to simulate the H_2/CO_2 separation in this work. Moreover, the loading effects of the high sorption gases (i.e., water vapor and CO_2) in carbon membranes were not included in the membrane model as their expected sorption will be significantly reduced at higher operating temperatures. It is also worth noting that the process reported for the purification of H_2 from a fermentation process by He et al. [33] is different from the SMR process in this work where the gas stream that comes out from the LTWGS reactor is above 200 °C and a high-pressure of 15–25 bar. In that work, a two-stage carbon membrane system including an H_2-selective membrane in the 1st-stage with a CO_2-selective membrane in the 2nd-stage was proposed to get a high purity of H_2 [33] due to the low H_2/CO_2 selectivity operated at low temperature, and using only H_2-selective carbon membrane was technically unfeasible. Moreover, dry feed gas (containing only H_2 and CO_2) was simulated as most of the previously reported carbon membranes cannot handle water vapor very well due to the pore blocking of the condensed water molecules inside pores. However, the high H_2-selective carbon membranes reported in this work can complete such separation requirements without the need for the CO_2-selective membrane. Moreover, the reported carbon membranes in this work provide good stability in humidified conditions (based on the durability testing results [30]). The process parameter optimization based on the experimental data obtained from the mixed gas permeation testing was conducted, and the sensitivity analysis on the process operating parameters such as required H_2 purity, and operating pressure and temperature was also investigated based on process simulation and cost estimation.

2.3.3. *Cost model*

Since the compressors and membrane units are the dominating cost in the membrane separation systems, as reported in previous work [34–36], capital cost estimation based on the major equipment of compressors and membrane units was investigated in this work, as is summarized in Table 3. The cost values are based on the 2018 Chemical Engineering Plant Cost Index (CEPCI) value of 603.1 and calculated from CAPCOST 2017 [37], which is only used for the estimation of major equipment (compressors) cost. The centrifugal compressors (450–3000 kW) with carbon steel materials were selected for this relatively moderate operating condition. The bare module cost (C_{BM}), which is calculated by the result of the purchase cost (C_p^0) of equipment in base conditions and a bare module factor (F_{BM}), is used for the compressor cost evaluation [37], as shown in Eq. (2),

$$C_{BM} = C_p^0 F_{BM} \tag{2}$$

Where C_p^0 is calculated by,

$$log_{10}\ C_p^0 = K_1 + K_2 log_{10}\ (A) + K_3 [log_{10}\ (A)]^2 \tag{3}$$

where A is the power of compressors. K_1, K_2, and K_3 are constant and equivalent to 2.289, 1.360, and −0.1027 for a centrifugal compressor [37].

The total module cost (C_{TM}) is evaluated by the values of 15% and 3% of the bare module cost (corresponding to the contingency costs and fees, respectively) as given in Eq. (4), and the grassroots cost (C_{GR}) can be further evaluated based on Eq. (5),

Table 3
Cost models and parameters for H_2 purification using CHFMs.

Category	Parameter	Value
Capital expenditure (CAPEX)	Membrane skid cost (C_M)	100 $/m^2
	Compressor grassroots cost (C_{GR})	Eq. 5
Annual operating expenditure (OPEX)	Electricity cost (*EC*)	0.05 $/kWh
	Labor cost (*LC*)	17 $/h[a]
Annual capital related cost (*CRC*)	0.2 C_{GR} + 0.28 C_M	
H_2 purification cost		Eq. 6
Other assumptions	Membrane lifetime	5 years
	Equipment lifetime	20 years
	Project lifetime	20 years
	Operating time	7500 h/year

[a] Based on 25 MMSCFD (1 MMSCFD = 1177.2 Nm^3/h) [39,40].

$$C_{TM} = 1.18 \sum_{i=}^{n} C_{BM} \tag{4}$$

$$C_{GR} = C_{TM} + 0.5 \sum_{i=}^{n} C_{BM,i}^{0} \tag{5}$$

where n represents the total number of pieces of equipment, and $C_{BM,i}^{0}$ is the bare module costs in the base conditions.

For the membrane unit, the membrane lifetime is assumed to 5 years, and the carbon membrane cost of 100 $\$/m^2$ was used [38], which includes the membrane material, module, and installation cost. It is worth noting that carbon membrane may face physical and/or chemical aging over a long operation period as reported in the previous work [30]. However, by applying regeneration, the membrane performance of both gas permeance and selectivity can be highly recovered, especially reach 95% of the original H_2/CO_2 selectivity as reported by Lei et al. [30]. Therefore, we assume that the membrane performance listed in Table 2 (based on experimental data) can be maintained in the whole membrane lifetime. However, a correction factor toward degradation during 5 years of operation might be applied in future work. Annual capital related cost (CRC) for the whole system is estimated to be 20% of the total grassroots cost of compressors and 28% of the membrane skid cost, which covers depreciation, interest, and equipment maintenance. For operating expenditure (OPEX), only electricity and labor cost are considered to simplify the cost estimation. Thus, the specific H_2 purification cost ($\$/Nm^3$ H_2 produced) was estimated by,

$$H_2 \ specific \ purification \ cost = \frac{CRC + OPEX}{annual \ H_2 \ productivity} \tag{6}$$

3. Results and discussion

3.1. H_2/CO_2 separation performance

Fig. 3 shows the separation performance as a function of testing temperature ranges from 25 °C to 110 °C under 10 bar with dry mixed gas (50 vol% H_2/50 vol% CO_2) feeding. In our recent work, both gas permeance and H_2/CO_2 selectivity were enhanced by increasing the operating temperature [30]. It should be noted that the higher operating temperatures can accelerate gas diffusion, which results in improved gas permeance. Simultaneously, the CO_2 adsorption will be limited at higher temperatures, which improves the H_2/CO_2 selectivity. For instance, the H_2 permeance of 25.9 GPU (1GPU = 3.35×10^{-10} mol/(s m^2 Pa)) and H_2/CO_2 selectivity of 30.8 were recorded at 25 °C. At 110 °C, the selectivity and H_2 permeance increased to 36.9 and 111 GPU, respectively, which are approximately 1.2 times and 4.3 times higher than that of 25 °C. The gas permeances obtained from the mixed gas permeation testing were used as the simulation basis. The apparent activation energies of H_2 and CO_2 are estimated to 16.7 kJ/mol and 14.7 kJ/mol based on the Arrhenius relationship given in Eq. (7),

$$\ln\left(\frac{P}{l}\right) = \ln\left(\frac{P_0}{l}\right) - \frac{E_a}{R}\frac{1}{T} \tag{7}$$

Due to the coexistence of both molecular sieving activate transport and selective surface flow transport for the CO_2 molecule, it presents a strong affinity with the carbon membrane surface. Thus, CO_2 can be more easily adsorbed along the pore wall compared to the less adsorbable H_2. The relatively lower apparent activation energy of CO_2 compared to H_2 indicates that the operating temperature provides a more significant effect on H_2 permeance. Based on the Arrhenius relationship, the membrane performances are extrapolated to higher operating temperatures (e.g., 150 and 200 °C), as depicted in Fig. 3. It can be found that the higher operating temperatures present the enhanced membrane performances of both H_2 permeance and H_2/CO_2 selectivity, which are preferable for industrial application. Therefore, the sensitivity analysis of operating temperature on the economic benefit of carbon membrane systems for H_2 purification is discussed in section 3.2. It should be noted that the membrane module was sealed by Loctite EA 3430 epoxy adhesive, which cannot withstand for a long time the conditions under the water-vapor contained gas stream at a temperature above 110 °C and 10 bar. Therefore, identifying a more suitable epoxy potting material for the higher temperature testing should be pursued in future work.

Since the gas stream after the LTWGS reactor contains water vapor (e.g., 20 vol%), it is essential to investigate the membrane separation performance and stability under humidified conditions. In our previous work, the developed CHFMs show a hydrophilic property and therefore have shown excellent stability under humidified conditions [30]. Fig. 4 shows the separation performance of the prepared CHFMs tested at various feed pressures using a fully-humidified gas mixture (50 vol% H_2/50 vol% CO_2). Specifically, the H_2 permeance drops with the increase of the total feed pressure, whereas the H_2/CO_2 selectivity increases. The prepared carbon membrane shows a lower performance (H_2 permeance of 73.2 GPU and H_2/CO_2 selectivity of 31.2) under humidified conditions compared with the testing results obtained under dried

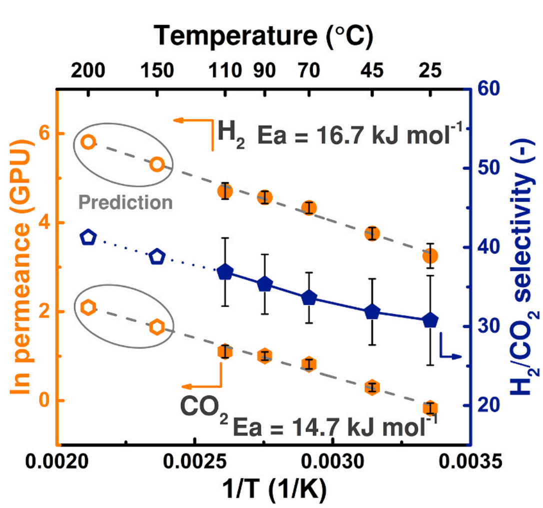

Fig. 3. Effects of operating temperature (25–110 °C) on separation performance (solid symbols) under 10 bar mixed gas (50 vol% H_2/50 vol% CO_2) with dry feeding. The predicted performances (hollow symbols) at 150 and 200 °C are obtained by the extrapolation based on the Arrhenius plots (gray dash lines).

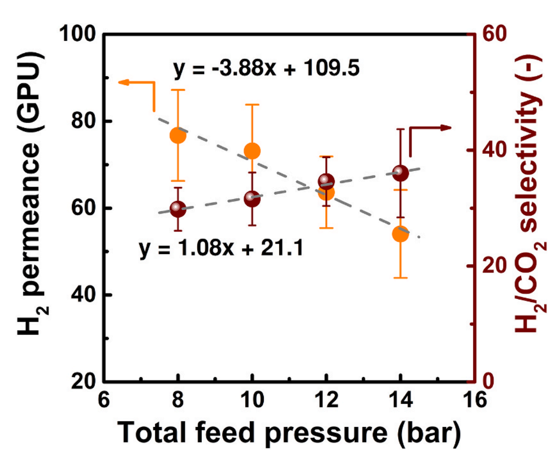

Fig. 4. Mixed gas separation performances using a 50 vol% H_2/50 vol% CO_2 gas mixture as a function of total feed pressure tested under 100% RH conditions at 90 °C (the gray dot lines give a linear fitting model for the relationship between the performance and total pressure.

conditions at 10 bar and 90 °C (see Fig. 3, with the corresponding H_2 permeance of 96.3 GPU and H_2/CO_2 selectivity of 35.3), which might be caused by the water sorption at the micropores of carbon matrix that hinders the diffusion of H_2 and CO_2 molecules. The sorption behavior of water molecules and carbon matrix as well as the interaction between water molecules and other permeating gases will be investigated in future work. By employing a linear regression model for the performance with the total feed pressure (see Fig. 4), the H_2 permeance and H_2/CO_2 selectivity were expanded to a wider pressure range for process simulation. It should be noted that the linear fitting may underestimate the H_2 permeance at much higher pressures (e.g., >20 bar) since the trend usually approaches a plateau at high pressure for CMS membranes [41]. Therefore, the simulations were only conducted at feed pressures of up to 20 bar.

3.2. Process optimization

Although the prepared carbon membrane shows good H_2/CO_2 separation performance at elevated temperatures and high pressures, as is documented above, the technological feasibility analysis for H_2 purification in an integrated WGS process at plant scale should be conducted by process simulation. The optimal operating condition and the sensitivity analysis of H_2 loss and H_2 purity and operating temperature are discussed in detail.

3.2.1. Effect of the 1st-stage feed pressure

The operating pressure could significantly affect the specific cost as there is a trade-off between the driving force and gas permeance when changing feed pressure. Specifically, a higher transmembrane pressure (requires higher energy for compressors) provides a higher driving force for gas permeation, resulting in a higher gas flux thereby leading to a reduced membrane area. However, as illustrated in Fig. 4, the higher transmembrane pressure will lead to reduced H_2 permeance, resulting in the requirement of additional membrane area to compensate for the performance loss. Thus, the membrane area (directly related to CAPEX) is a function of operating pressure. Correspondingly, the operating pressure can be optimized to minimize the specific cost by balancing CAPEX and OPEX. Considering the outlet pressure of an LTWGS process is normally around 10–20 bar, the feed pressure for the 1st-stage membrane unit can be easily controlled. In this part, the total H_2 loss is controlled at below 10% and H_2 purity is set to 99.5 vol%, as is depicted in Fig. 2 and listed in Table 4. Scenario A is to investigate the effect of the 1st-stage feed pressure on the processing cost.

When the 1st-stage feed pressure is increased from 10 to 20 bar, the required membrane area shows a minimum value at 16 bar, while the power demand for the compressors is slightly decreased. As a result, the specific cost for producing H_2 follows the same trend as the membrane cost, as is shown in Fig. 5. Since the 2nd-stage feed pressure and the 1st-stage permeate pressure are kept constant, the required membrane area for the 2nd-stage membrane unit is almost constant. However, by adjusting the 1st-stage feed pressure, the “trade-off” between the driving force and H_2 permeance leads to a parabolic dependence of the membrane area on the 1st-stage feed pressure. The higher transmembrane pressure applied in the 1st-stage membrane unit also produces a relatively higher purity of H_2 in the permeate, which leads to a reduced recycling rate. Thus, the power demand for the compression of the 1st-stage permeate gas before feeding to the 2nd-stage membrane unit will be slightly reduced, as shown in Fig. 5. Based on these factors, the optimal specific cost for producing 99.5% H_2 is 0.0157 \$/Nm^3 when the 1st-stage feeding pressure is operated at 16 bar. It should be noted that the high-pressure vent gas at the 1st-stage retentate can be expanded to recover work, and potentially reduce the overall power demand - this is however not included in the current study.

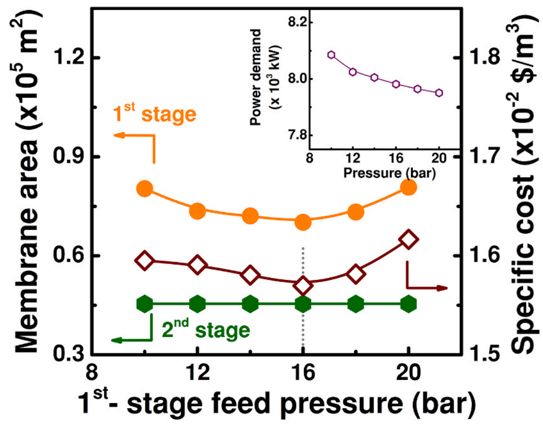

Fig. 5. The influence of the 1st-feed pressure on the required membrane area, specific cost, and power demand (the inserted figure).

Table 4
Separation scenarios for the optimization of the operating pressure.

Scenario	1st-stage feed pressure (bar)	2nd-stage feed pressure (bar)	1st-stage permeate pressure (bar)	H_2 loss (%)	H_2 purity[a] (vol%)
A	10–20	10	1	10	99.5
B	Optimized from scenario A	4–16	1	10	99.5
C	Optimized from scenario A	Optimized from scenario B	1–4	10	99.5

[a] Dry-based gas composition.

3.2.2. Effect of the 2nd-stage feed pressure

When applying the optimized feed pressure of the 1st-stage membrane unit at 16 bar, the 2nd-stage feed pressure was optimized (as scenario B depicted in Table 4). Fig. 6 shows the effects of the 2nd-stage feed pressure on the key parameters, such as membrane area, power demand, CRC, and specific cost. The required membrane area for the 1st-stage membrane unit is almost constant (with a slight reduction from 70800 to 70000 m^2) due to the fixed feed pressure of 16 bar. However, the required membrane area for the 2nd-stage unit is reduced from 103000 to 43000 m^2 when the pressure is increased from 4 to 16 bar. It is expected that a higher feed pressure increases the driving force, and therefore the required membrane area for the 2nd-stage unit is reduced, as shown in Fig. 6a. On the other hand, the higher pressure ratio between the 2nd-stage feed and 1st-stage permeate stream, caused by the increased 2nd-stage feed pressure, leads to more extensive power demand for the inter-stage compressors (i.e., K-1 in Fig. 2), which increases the compressor capital cost (i.e., additional compressors may be required) and the OPEX. Due to the combination of these two opposing factors (the reduced membrane capital cost and the increase of compressor related cost), the specific cost for H_2 purification decreases initially and then followed by an increase when the 2nd-stage feed pressure is above 6 bar, as demonstrated in Fig. 6b.

3.2.3. Effect of the 1st-stage permeate pressure

The specific cost was further optimized by adjusting the 1st-stage permeate pressure, as illustrated in Fig. 7 (the 1st- and 2nd-stage feed pressure were kept at 16 bar and 6 bar, respectively, scenario C). The required membrane area of the 2nd-stage membrane unit is almost constant (~68000 m^2) because the feed pressure and H_2 purity were kept constant when adjusting the 1st-stage permeate pressure. Although the lower transmembrane pressure at the 1st-stage unit caused by the higher permeate pressure requests a larger membrane area to fulfill the required H_2 loss (resulting in a higher membrane skid cost), the power demand for the compression of the permeate stream to the 2nd-stage

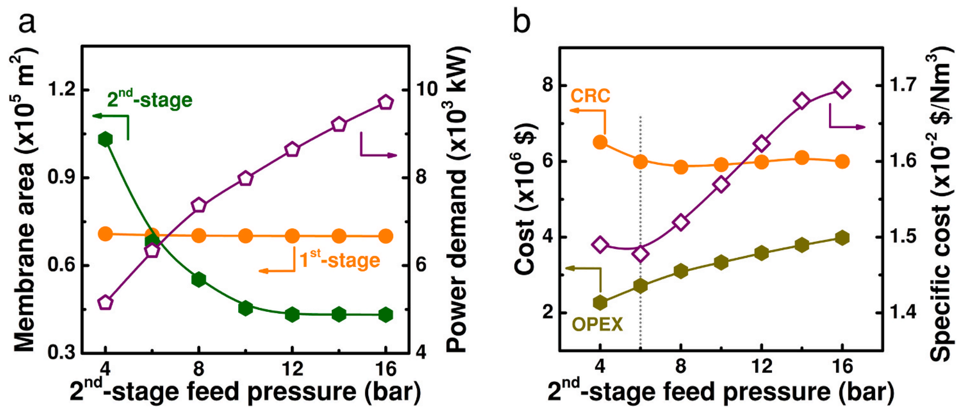

Fig. 6. The influence of the 2nd-stage feed pressure on the, a) membrane area and power demand, and b) CRC, OPEX, and specific cost.

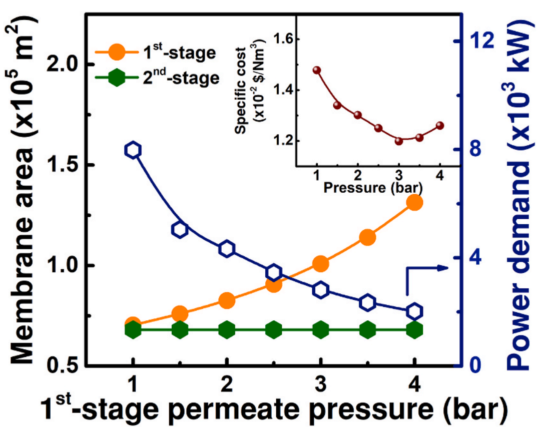

Fig. 7. The influence of the 1st-stage permeate pressure on the membrane area, power demand, and specific cost.

unit is however reduced (see Fig. 7) due to the lower pressure ratio. As a result, both the number of compressors and the OPEX decrease afterward. Thus, a minimum specific hydrogen purification cost of 0.012 \$/Nm^3 is obtained at the 1st-stage permeate pressure of 3 bar by balancing the membrane unit cost and the compressor related cost.

3.3. Sensitivity analysis of H_2 loss and purity

Based on the above optimized operating pressures for the two-stage membrane units, the techno-economic analysis of the H_2 purification process by studying the H_2 loss and purity were analyzed, as is listed in Table 5 and Fig. 8. Scenario D and E are used to investigate the influence of H_2 loss and H_2 purity, respectively. At a low H_2 loss of 3%, a large membrane area is needed to achieve a high H_2 penetration in the 1st-stage unit, and a high gas volume from the 2nd-stage retentate needs to be recycled, which results in increased power demand for the compressors. As a result, the total membrane area and the power consumption increase. As shown in Fig. 8a, when the H_2 loss in the 1st-stage retentate increases from 3% to 15% (the H_2 recovery reduces from 97% to 85%), the required total membrane area is reduced by 43.7% from 261000 to 147000 m^2, and the power consumption is reduced by 47.9% from 4800 to 2500 kW (Fig. 8b). Correspondingly, the specific H_2 production cost drops from 0.0174 to 0.0113 \$/Nm^3, caused by the decrease of CRC and OPEX (Fig. 8b). However, the higher H_2 loss leads to lower H_2 productivity, which is not desirable in an industrial process. Thus, a suitable H_2 loss (or H_2 recovery) should be essentially considered when designing and operating a real-life membrane system.

Table 5
Simulation scenarios of varying H_2 loss and purity under the optimized pressures.

Scenario	H_2 loss (%)	H_2 purity (vol%)	1st-stage feed pressure (bar)	1st-stage permeate pressure (bar)	2nd-stage feed pressure (bar)
D	3–15	99.5	16	3	6
E	10	99–99.8			

On the other hand, product purity is another crucial parameter for process design as the H_2 purity may differ for the various downstream applications. Fig. 8c and d illustrate the parameters (such as required membrane area, compressors power demand, and cost) as a function of H_2 purity at a given H_2 loss of 10% and the optimized pressures. When the required H_2 purity increases, the higher flow rate needs to be recycled back to the 1st-stage membrane unit, which indicates that less membrane area at the 2nd-stage is required to achieve the given target for H_2 purity. Besides, the higher flow rate of the mixed feed and recycling streams at the 1st-stage unit means a larger production capacity, which results in increased membrane areas (Fig. 8c) and higher power demands for compressors (Fig. 8d). Thus, the required membrane area of the two-stage membrane units shows an opposite trend, leading to a minimum total membrane area and CRC at an H_2 purity of 99.5 vol%, as shown in Fig. 8c and d. However, when the H_2 purity requirement exceeds 99.5 vol%, the 1st-stage membrane area and power demand for compressors increase dramatically due to a large recycling volume, which brings to a much higher specific cost. For example, the specific cost increases from 0.012 to 0.0158 \$/Nm^3 when the H_2 purity requirement was set from 99.5 to 99.8 vol%. This indicates that such a carbon membrane system may still not be cost-effective for producing very high purity hydrogen compared to other technologies, as reported by other works [26,42]. To address this challenge, the development of highly selective membrane materials together with high gas permeance should be further pursued.

3.4. Sensitivity analysis of operating temperature

The great advantage of CMS membranes for H_2/CO_2 separation is the feasibility for the enhancement of separation performance (both in gas permeance and H_2/CO_2 selectivity) by elevating the operating temperature, as illustrated in Fig. 3. Based on the Arrhenius plot of the experimental data obtained at the feed and permeate pressure of 10 bar and 1 bar, the sensitivity analysis of the operating temperature at an expanded range of 110–200 °C was investigated for producing high purity H_2. The H_2 loss was controlled at 10%, while the H_2 purity was varied from 99.5 to 99.95 vol%. As shown in Fig. 9a, the CRC and OPEX for relatively low H_2 purity requirement (e.g., <99.7 vol%) are approximately the same when operated at different temperatures, which indicates that the

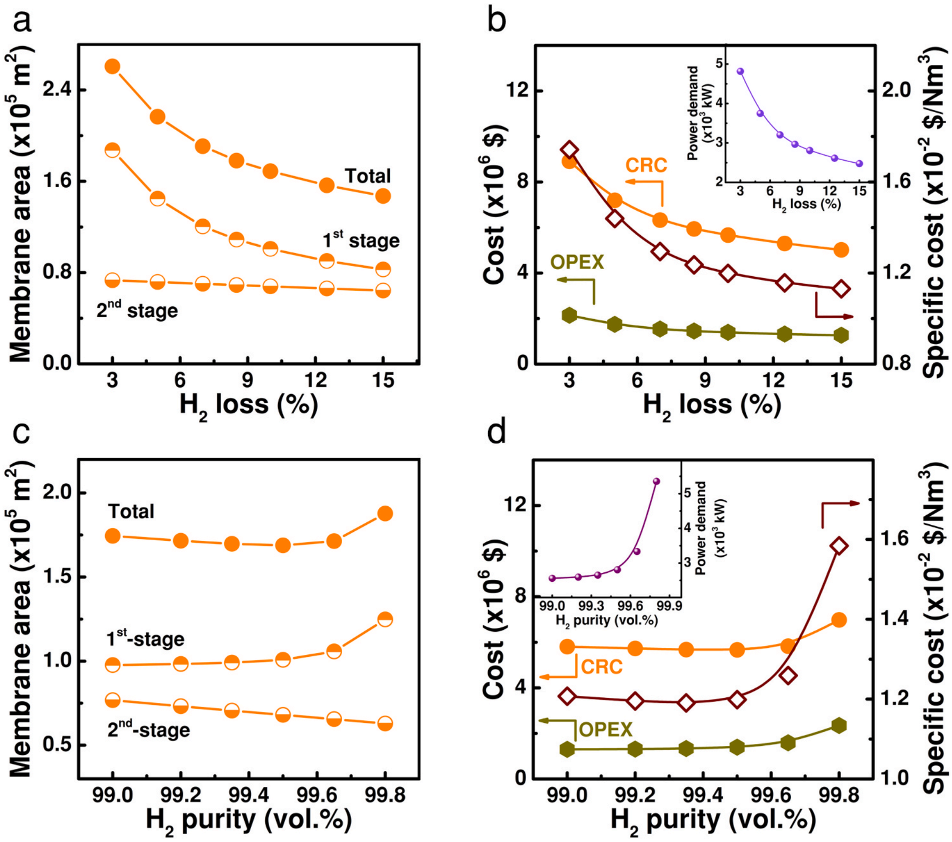

Fig. 8. Dependence of membrane area, power demand and specific cost on the a, b) H_2 loss, and c, d) H_2 purity.

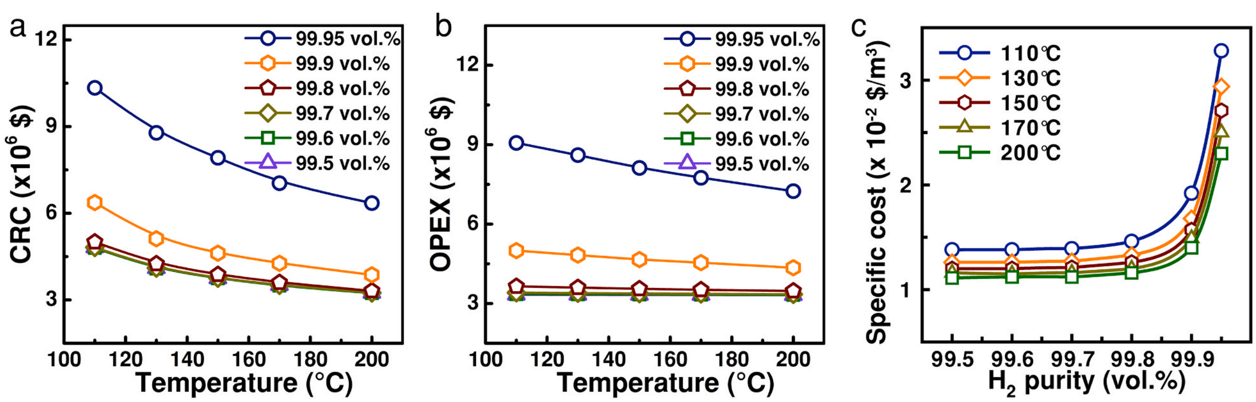

Fig. 9. Dependence of a) CRC, b) OPEX, and c) specific cost on the operating temperature and H_2 purity.

carbon membranes with an H_2/CO_2 selectivity ~ 40 can easily produce 99.7 vol% H_2 using a two-stage system without recycling. However, when the separation target for H_2 purity increases from 99.8 to 99.95 vol %, the CRC and OPEX increase dramatically, indicating that a larger membrane area and higher power demand for compressors are needed. On the other hand, due to the enhanced H_2 permeance and H_2/CO_2 selectivity at higher temperatures, the CRC and OPEX are reduced at a given H_2 purity by elevating temperature. Fig. 9c shows the specific cost for producing high purity H_2 up to 99.95 vol%, which also implies that pursuing very high purity hydrogen will increase the specific cost dramatically. However, it should be noted that the selling price for the higher purity product also increases, which may partially offset the increased production cost. Therefore, further optimization can be conducted in a real industrial case in future work.

4. Conclusions

In summary, asymmetric carbon hollow fiber membranes were prepared from biomaterial of cellulose and present remarkable H_2/CO_2 mixed gas separation performances at high temperature and high pressure and fully-humified conditions. Due to the weakened CO_2 sorption at high temperatures, the membranes showed enhanced H_2/CO_2 selectivity at elevated operating temperatures, which is favorable for H_2 purification in the SMR + WGS process. The techno-economic feasibility analysis for the prepared membranes for hydrogen purification was systematically investigated by HYSYS simulation integrated with an in-house membrane model (ChemBrane). A two-stage membrane system with 6000 kmol/h capacity, containing a recycling stream from the 2nd-stage retentate to the 1st-stage feeding stream, was designed to produce high purity hydrogen. It was found that the operating pressure could significantly affect the specific H_2 purification cost because of a "trade-off" between the driving force and gas permeance. For the developed carbon membranes, the specific cost reached a minimum of 0.012 $/Nm^3 when the 1st-stage feed pressure, the 1st-stage permeate pressure, and the 2nd-feed pressure were optimized at 16 bar, 3 bar, and 6 bar, respectively. However, the process simulation results demonstrate that achieving very high H_2 purity is challenging for membrane systems to be economically competitive. Due to the limitation of H_2/CO_2 selectivity, producing high purity product (e.g., >99.8 vol%) requires a high H_2 recycling rate, which will dramatically increase both capital investments (large membrane area and more compressors) and OPEX (high energy consumption). Elevating operating temperature could significantly save the separation cost due to the simultaneously enhanced H_2 permeance and H_2/CO_2 selectivity, and provide a possibility to produce >99.95 vol% H_2 product. This also implies that the development of highly selective membrane materials should be further pursued to achieve a high-purity product at a lower cost.

Author statement

Linfeng Lei: Methodology, Investigation, Writing-original draft. Arne Lindbråthen: Methodology, Manuscript review and editing. Magne Hillestad: Supervision, Manuscript review and editing. Xuezhong He: Investigation, Supervision, Project administration, Manuscript writing, review and editing.

Declaration of competing interest

The authors declare that they have no known competing financial interests or personal relationships that could have appeared to influence the work reported in this paper.

Acknowledgment

The authors would like to acknowledge the Research Council of Norway through the CO2Hing project (267615), and the Startup fund from Guangdong Technion Israel Institute of Technology (GTIIT) for funding this work.

References

[1] W.-H. Chen, C.-Y. Chen, Water gas shift reaction for hydrogen production and carbon dioxide capture: a review, Appl. Energy 258 (2020) 114078.
[2] N.W. Ockwig, T.M. Nenoff, Membranes for hydrogen separation, Chem. Rev. 107 (2007) 4078–4110.
[3] L. Wei, J. Yu, Y. Huang, Silver coating on porous stainless steel substrate and preparation of H_2-permeable palladium membranes, Int. J. Hydrogen Energy 38 (2013) 10833–10838.
[4] S. Sircar, T.C. Golden, Purification of hydrogen by pressure swing adsorption, Separ. Sci. Technol. 35 (2000) 667–687.
[5] K. Atsonios, K.D. Panopoulos, A. Doukelis, A.K. Koumanakos, E. Kakaras, T. A. Peters, Y.C. van Delft, 1 - introduction to palladium membrane technology, in: Palladium Membrane Technology for Hydrogen Production, Carbon Capture and Other Applications, Woodhead Publishing, 2015, pp. 1–21.
[6] L. Zhu, M.T. Swihart, H. Lin, Unprecedented size-sieving ability in polybenzimidazole doped with polyprotic acids for membrane H_2/CO_2 separation, Energy Environ. Sci. 11 (2018) 94–100.
[7] M. Shan, X. Liu, X. Wang, I. Yarulina, B. Seoane, F. Kapteijn, J. Gascon, Facile manufacture of porous organic framework membranes for precombustion CO_2 capture, Science Advances 4 (2018), eaau1698.
[8] H.W. Kim, H.W. Yoon, S.-M. Yoon, B.M. Yoo, B.K. Ahn, Y.H. Cho, H.J. Shin, H. Yang, U. Paik, S. Kwon, J.-Y. Choi, H.B. Park, Selective gas transport through few-layered graphene and graphene oxide membranes, Science 342 (2013) 91.
[9] M. Yu, H.H. Funke, R.D. Noble, J.L. Falconer, H2 separation using defect-free, inorganic composite membranes, J. Am. Chem. Soc. 133 (2011) 1748–1750.
[10] Y. Peng, Y. Li, Y. Ban, H. Jin, W. Jiao, X. Liu, W. Yang, Metal-organic framework nanosheets as building blocks for molecular sieving membranes, Science 346 (2014) 1356.
[11] Y. Peng, Y. Li, Y. Ban, W. Yang, Two-dimensional metal–organic framework nanosheets for membrane-based gas separation, Angew. Chem. Int. Ed. 56 (2017) 9757–9761.
[12] H.-H. Tseng, C.-T. Wang, G.-L. Zhuang, P. Uchytil, J. Reznickova, K. Setnickova, Enhanced H_2/CH_4 and H_2/CO_2 separation by carbon molecular sieve membrane coated on titania modified alumina support: effects of TiO_2 intermediate layer preparation variables on interfacial adhesion, J. Membr. Sci. 510 (2016) 391–404.
[13] L.M. Robeson, The upper bound revisited, J. Membr. Sci. 320 (2008) 390–400.
[14] M.-B. Hagg, J.A. Lie, A. Lindbrathen, Carbon molecular sieve membranes. A promising alternative for selected industrial applications, Ann Ny Acad Sci 984 (2003) 329–345.
[15] L. Lei, A. Lindbråthen, X. Zhang, E.P. Favvas, M. Sandru, M. Hillestad, X. He, Preparation of carbon molecular sieve membranes with remarkable CO_2/CH_4 selectivity for high-pressure natural gas sweetening, J. Membr. Sci. 614 (2020) 118529.
[16] L. Lei, A. Lindbråthen, M. Hillestad, M. Sandru, E.P. Favvas, X. He, Screening cellulose spinning parameters for fabrication of novel carbon hollow fiber membranes for gas separation, Ind. Eng. Chem. Res. 58 (2019) 13330–13339.
[17] X. He, M.-B. Hägg, Hollow fiber carbon membranes: from material to application, Chem. Eng. J. 215–216 (2013) 440–448.
[18] N. Bhuwania, Y. Labreche, C.S.K. Achoundong, J. Baltazar, S.K. Burgess, S. Karwa, L. Xu, C.L. Henderson, P.J. Williams, W.J. Koros, Engineering substructure morphology of asymmetric carbon molecular sieve hollow fiber membranes, Carbon 76 (2014) 417–434.
[19] Y. Cao, K. Zhang, O. Sanyal, W.J. Koros, Carbon molecular sieve membrane preparation by economical coating and pyrolysis of porous polymer hollow fibers, Angew. Chem. Int. Ed. 58 (2019) 12149–12153.
[20] S. Fu, E.S. Sanders, S.S. Kulkarni, W.J. Koros, Carbon molecular sieve membrane structure–property relationships for four novel 6FDA based polyimide precursors, J. Membr. Sci. 487 (2015) 60–73.
[21] D.-Y. Koh, B.A. McCool, H.W. Deckman, R.P. Lively, Reverse osmosis molecular differentiation of organic liquids using carbon molecular sieve membranes, Science 353 (2016) 804.
[22] L.I.B. David, A.F. Ismail, Influence of the thermastabilization process and soak time during pyrolysis process on the polyacrylonitrile carbon membranes for O_2/N_2 separation, J. Membr. Sci. 213 (2003) 285–291.
[23] M. Cao, L. Zhao, D. Xu, R. Ciora, P.K.T. Liu, V.I. Manousiouthakis, T.T. Tsotsis, A carbon molecular sieve membrane-based reactive separation process for pre-combustion CO_2 capture, J. Membr. Sci. 605 (2020) 118028.
[24] A. Harale, H.T. Hwang, P.K.T. Liu, M. Sahimi, T.T. Tsotsis, Experimental studies of a hybrid adsorbent-membrane reactor (HAMR) system for hydrogen production, Chem. Eng. Sci. 62 (2007) 4126–4137.
[25] D. Parsley, R.J. Ciora, D.L. Flowers, J. Laukaitaus, A. Chen, P.K.T. Liu, J. Yu, M. Sahimi, A. Bonsu, T.T. Tsotsis, Field evaluation of carbon molecular sieve membranes for the separation and purification of hydrogen from coal- and biomass-derived syngas, J. Membr. Sci. 450 (2014) 81–92.
[26] C. Zhang, W.J. Koros, Ultraselective carbon molecular sieve membranes with tailored synergistic sorption selective properties, Adv. Mater. 29 (2017) 1701631.
[27] L. Xu, M. Rungta, W.J. Koros, Matrimid® derived carbon molecular sieve hollow fiber membranes for ethylene/ethane separation, J. Membr. Sci. 380 (2011) 138–147.
[28] S.C. Rodrigues, M. Andrade, J. Moffat, F.D. Magalhães, A. Mendes, Carbon membranes with extremely high separation factors and stability, Energy Technol. 7 (2019) 1801089.
[29] S. Sá, J.M. Sousa, A. Mendes, Steam reforming of methanol over a $CuO/ZnO/Al_2O_3$ catalyst part II: a carbon membrane reactor, Chem. Eng. Sci. 66 (2011) 5523–5530.
[30] L. Lei, F. Pan, A. Lindbråthen, X. Zhang, M. Hillestad, Y. Nie, L. Bai, X. He, M. D. Guiver, Carbon hollow fiber membranes for a molecular sieve with precise-cutoff ultramicropores for superior hydrogen separation, Nat. Commun. 12 (2021) 268.
[31] X. He, Y. Chu, A. Lindbråthen, M. Hillestad, M.-B. Hägg, Carbon molecular sieve membranes for biogas upgrading: techno-economic feasibility analysis, J. Clean. Prod. 194 (2018) 584–593.
[32] Y. Chu, A. Lindbråthen, L. Lei, X. He, M. Hillestad, Mathematical modeling and process parametric study of CO_2 removal from natural gas by hollow fiber membranes, Chem. Eng. Res. Des. 148 (2019) 45–55.
[33] X. He, Techno-economic feasibility analysis on carbon membranes for hydrogen purification, Separ. Purif. Technol. 186 (2017) 117–124.
[34] X. He, C. Fu, M.-B. Hägg, Membrane system design and process feasibility analysis for CO_2 capture from flue gas with a fixed-site-carrier membrane, Chem. Eng. J. 268 (2015) 1–9.
[35] X. He, M.-B. Hägg, T.-J. Kim, Hybrid FSC membrane for CO_2 removal from natural gas: experimental, process simulation, and economic feasibility analysis, AIChE J. 60 (2014) 4174–4184.
[36] X. He, I. Kumakiri, M. Hillestad, Conceptual process design and simulation of membrane systems for integrated natural gas dehydration and sweetening, Separ. Purif. Technol. 247 (2020) 116993.
[37] R. Turton, R.C. Bailie, W.B. Whiting, J.A. Shaeiwitz, Analysis, Synthesis and Design of Chemical Processes, fifth ed., Pearson Education, 2018.
[38] L. Lei, L. Bai, A. Lindbråthen, F. Pan, X. Zhang, X. He, Carbon membranes for CO_2 removal: status and perspectives from materials to processes, Chem. Eng. J. 401 (2020) 126084.
[39] X. He, M.-B. Hägg, Energy efficient process for CO_2 capture from flue gas with novel fixed-site-carrier membranes, Energy Procedia 63 (2014) 174–185.

[40] X. Zhang, X. He, T. Gundersen, Post-combustion carbon capture with a gas separation membrane: parametric study, capture cost, and exergy analysis, Energy Fuel. 27 (2013) 4137–4149.
[41] C. Zhang, G.B. Wenz, P.J. Williams, J.M. Mayne, G. Liu, W.J. Koros, Purification of aggressive supercritical natural gas using carbon molecular sieve hollow fiber membranes, Ind. Eng. Chem. Res. 56 (2017) 10482–10490.
[42] G. Bernardo, T. Araújo, T. da Silva Lopes, J. Sousa, A. Mendes, Recent advances in membrane technologies for hydrogen purification, Int. J. Hydrogen Energy 45 (2020) 7313–7338.